ADVANCED THEORY AND SIMULATIONS
www.advtheorysimul.com

Computational Insights into the Stability, Mechanical, Optoelectronic, and Thermoelectric Characteristics Investigation on Lead-Based Double Perovskites of $(Cs_2, K_2, Rb_2)PbCl_6$: Promising Candidates for Optoelectronic Applications

M. A. Ghebouli, K. Bouferrache, Faisal Katib Alanazi, B. Ghebouli, and M. Fatmi**

Lead-based double perovskites are studied in the cubic phase using the generalized gradient approximation and the modified Becke–Johnson (mBJ-GGA) functionals as implemented in the Wien2K code. Goldschmidt tolerance factor and octahedral factor, formation enthalpy, and formation energy translate the structural, chemical, and thermodynamic stability of double perovskites studied. Phonon band structures and elastic moduli ensure the dynamic and mechanical stability of $(Cs_2, K_2, Rb_2)PbCl_6$. An intermediate band appears in the conduction band and the fundamental transition takes place between 3p-Cl state and 6p-Pb site. The refractive index of double perovskites $(Cs_2, K_2, Rb_2)PbCl_6$ in the visible and ultraviolet light hold a huge advantage for solar cell applications. The wide dielectric constant of double perovskites under study makes them capable for absorbing energy between 1 and 5 eV, and are suitable for solar power applications. $(Cs_2, K_2, Rb_2)PbCl_6$ have positive Seebeck coefficient, which reveals that p-type charge carriers are dominant for enhancing their performance. Cs_2PbCl_6 has positive thermal conductivity for both n-type and p-type character. $(K_2, Rb_2)PbCl_6$ have positive thermal conductivity for n-type character. The complete analysis reveals that they are potentially significant candidates for future solar cells and energy harvesting devices.

1. Introduction

Lead in double perovskites materials, as Pb is a well-known heavy metal. Double perovskites based on lead and halides have attracted researchers to inorganic materials, which tend to undergo structural phase transitions, accompanied by changes in symmetry and physical properties. Improving the flexibility of lead-based perovskites for optoelectronic applications faces instability due to the use of organic components in the perovskite structure and toxicity due to Pb. Pb-Lead halide perovskites show exceptional photoelectric properties, due to their tunable bandgap and high photoluminescence quantum yield (PLQY).[1–3] A large series of lead-free perovskites with different molecular formulas and stable dimensions are needed to overcome these drawbacks. Lead-free double halide perovskite based on (Cs, K, Rb) has recently received significant attention. Gourji et al. present the challenges encountered by this type of perovskite and their applications, particularly in photovoltaïcs, as well as the effect of metal dopants on their performance.[4] The problem of lead toxicity in double perovskites materials, which work efficiently

M. A. Ghebouli, M. Fatmi
Research Unit on Emerging Materials (RUEM)
University Ferhat Abbas of Setif 1
Setif 19000, Algeria
E-mail: m.fatmi@univ-setif.dz

M. A. Ghebouli
Department of Chemistry
Faculty of Sciences
University of Mohamed Boudiaf
M'sila 28000, Algeria

K. Bouferrache
Department of Physics
Faculty of Sciences
University of Mohamed Boudiaf
M'sila 28000, Algeria

F. K. Alanazi
Department of Physics
College of Sciences
Northern Border University
Arar 73222, Saudi Arabia
E-mail: Fisal.alanazi@nbu.edu.sa

B. Ghebouli
Laboratory for the Study of Surfaces and Interfaces of Solid Materials (LESIMS)
University Ferhat Abbas of Setif 1
Setif 19000, Algeria

The ORCID identification number(s) for the author(s) of this article can be found under https://doi.org/10.1002/adts.202400938

DOI: 10.1002/adts.202400938

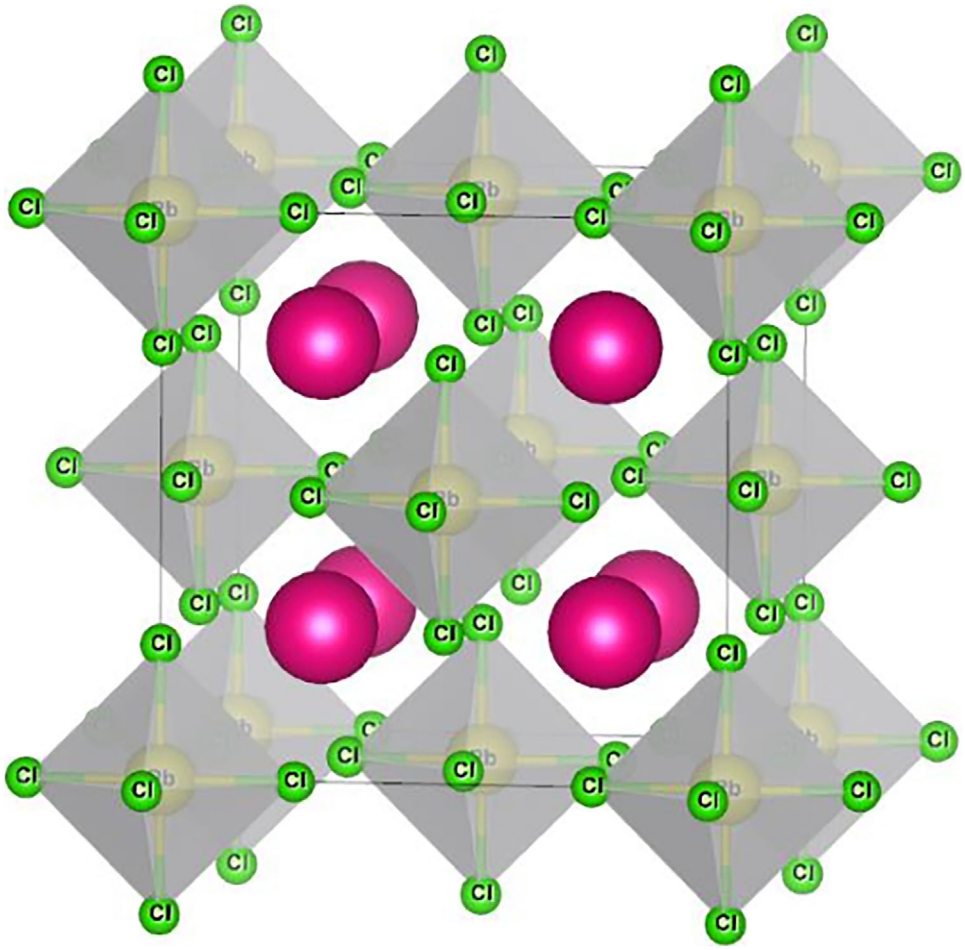

Figure 1. The crystal structure of $(Cs_2, K_2, Rb_2)PbCl_6$ in the cubic phase. *Cl* atom (green color), (*Cs, K, Rb*) (gray color), and *Pb* (magenta color).

is solved by a choice of double perovskites $(Cs_2, K_2, Rb_2)PbCl_6$, which have reduced lead contents. Inorganic Pb-lead halide perovskites are candidate materials for optoelectronic devices due to their excellent photoelectric properties, such as narrow emission, tunable emission wavelength in the visible spectrum, high mobility of charge carriers, and adequate bandgap.[5–8] The advantages of optical characteristics and semiconductors appear in various optoelectronic applications, such as light-emitting diodes, solar cells, photodetectors, lasers.[9–13] However, there are few drawbacks regarding lead-based halide perovskites in photovoltaïc applications, which need to be resolved in order to achieve large-scale application.[14] Ibrahim H. Al-Lehyani studies structure and electronic properties of $Cs_2Pb(Cl_6, I_6)$ using density functional theory as implemented in the pseudopotential-based package Quantum ESPRESSO.[15] Stability, storage performance, and release of elemental chlorine in vacancy-ordered chloride perovskites Cs_2PbCl_6, Rb_2PbCl_6, Rb_2PbI_6, $(NH_4)_2PbCl_6$, and $Cs_4Sb_2Cl_{12}$, were studied.[16]

CsPbX (*X = Cl, Br, I*) were synthesized on a mica substrate and an experimental study of the structure and optical properties was carried out.[17] The structural and optoelectronic properties of lead-based double perovskites Cs_2PbX_6 (*X = Cl, Br, I*) were computed using Vienna ab initio Simulation Package.[18] Cs_2PbX (*X = Cl, Br, I*) double perovskites have direct bandgap (0.45–2.54 eV) and large absorption coefficients 5.95×10^5 cm^{-1}, which are suitable for solar cell applications.[19] The results collected from this study on structure, mechanical, optoelectronic, and thermoelectric characteristics of $(Cs_2, K_2, Rb_2)PbCl_6$ prove that these double perovskites are suitable for solar cells. The stability of these materials is ensured by the study of optimization energy, formation enthalpy, and phonon spectra. The optimal light absorption in the infrared (IR) region and the bandgap values reflect the use of these compounds in optoelectronic devices. The transport characteristics are examined in terms of figure of merit, electrical conductivity, thermal conductivity, and Seebeck coefficient. Our results are useful for future experimental research for applications related to renewable energy devices.

2. Computational Method

The computation was carried out using the full potential linearized augmented plane wave (FP-LAPW) plus local orbitals as implemented in the WIEN2k code.[20] The maximum cutoff wavenumber K_{max} in the series of plane waves used inside the

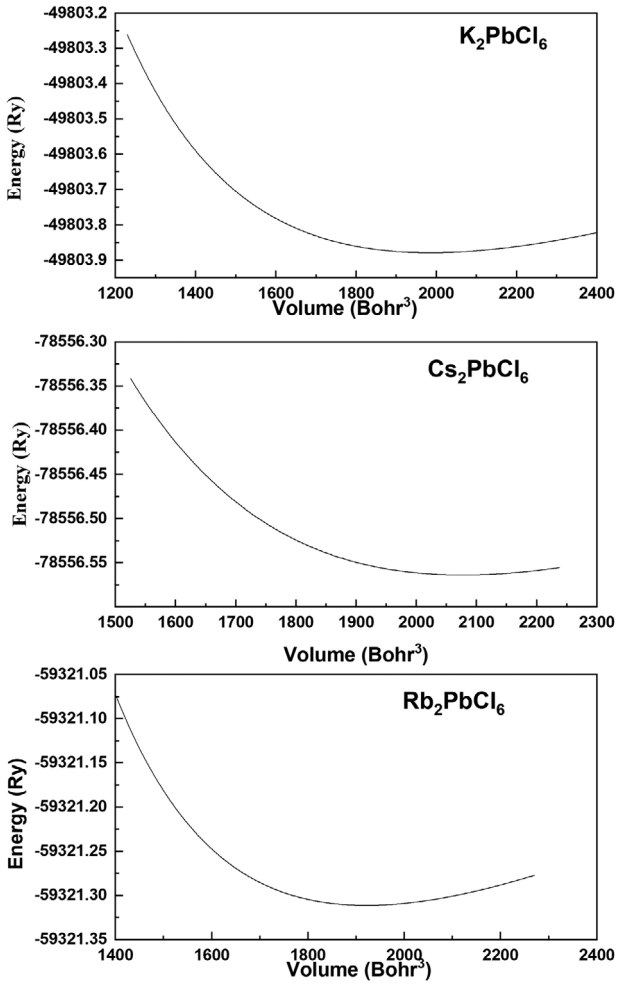

Figure 2. Optimization energy as a function of volume for $(Cs_2, K_2, Rb_2)PbCl_6$.

atomic spheres to describe the interstitials is set at 4. The corresponding cutoff energy $R_{MT}.K_{max}$ is selected as 9 Ry. The muffin tin sphere radius (R_{MT}) is the smallest atomic radius used for the density functional theory (DFT) calculations in a way to ensure no charge leakage from the core. The study is carried out for the simple cubic phase of the materials. The lattice constant is optimized usingBirch–Murnaghan's equation of state.[21] The generalized gradient approximation (GGA)[22] followed by the most accurate mBJ-GGA[23] are used as exchange potentials for self-consistency

Table 2. Bond lengths of nearest neighbors for $(Cs_2, K_2, Rb_2)PbCl_6$.

Bond	K_2PbCl_6	Cs_2PbCl_6	Rb_2PbCl_6
A—Pb [Å]	4.777	4.51	4.414
A—Cl [Å]	3.519	4.507 Exp.	4.416 Exp.
Pb—Cl [Å]	3.682 Exp.	4.43[15]	3.604
	2.196	3.685	3.606 Exp.
		3.682 Exp.	2.489
		2.471	2.491 Exp.
		2.47 Exp.	
		2.54[15]	

approximations. GGA-mBJ method takes the core electrons inside the atom as fully relativistic, while considering the valence electrons as semirelativistic. The number of *k*-points are set at $k = 5000\ cm^{-1}$, with the k_{mesh} $12 \times 12 \times 12$ in the first Brillouin zone. The R_{MT} of *K, Cs, Rb*, and *Pb* is 2.5. While the R_{MT} of *Cl* in K_2PbCl_6, Cs_2PbCl_6, and Rb_2PbCl_6 is 2.15, 2.19, and 2.18, respectively.

3. Results and Discussions

3.1. Ground State Parameters

The crystal structure of $(Cs_2, K_2, Rb_2)PbCl_6$ in the cubic phase with four basic unit cells is shown in **Figure 1**. The magenta circles represent the (*Cs, K, Rb*) atoms, the green ones are the halogen atoms and the lead atoms are locked inside the octahedra. Structural stability is studied based on optimization energy as a function of volume for $(Cs_2, K_2, Rb_2)PbCl_6$ as presented in **Figure 2**. The lattice constant and the position of the chlorine ion (u, 0, 0) describe the geometric appearance of the structure. The atomic positions are 8*K*, 8*Cs*, 8*Rb* (0.25, 0.25, 0.25), 4*Pb* (0, 0, 0), and 24 *Cl* (0.2407, 0, 0). **Table 1** lists the lattice constant, bulk modulus and its pressure derivative and the minimum energy for these compounds. It is reported that minimum energy confirms that stability is more pronounced following the sequence $Cs \rightarrow Rb \rightarrow K$. The computed lattice constant of Cs_2PbCl_6 and Rb_2PbCl_6 are in good agreement with their experimental and theoretical values cited in the literature.[19,24] The deviation between theoretical and experimental values is less than 0.9%. Fang et al. prove that distortions are the only cause of phase variations in perovskites.[25] Octahedral distortions in perovskite structures are a determining factor in their stability. Indeed, increasing octahedral distortions reduces the free energy of the system, and therefore improves structural

Table 1. Lattice constant, bulk modulus, and its pressure derivative and the minimum energy for $(Cs_2, K_2, Rb_2)PbCl_6$.

	a [Å]	*B* [GPa]	B'	E_{form} [Ry]
K_2PbCl_6	10.539	9.10	5.03	−49 803.87
Cs_2PbCl_6	10.416	13.59	5.36	−78 556.56
	Exp. 10.415[24]	9.21[18]		
	Cal. 10.54[19]			
Rb_2PbCl_6	10.195	23.11	6.53	−59 321.31
	Exp. 10.195[24]	Cal. 33.97[18]		

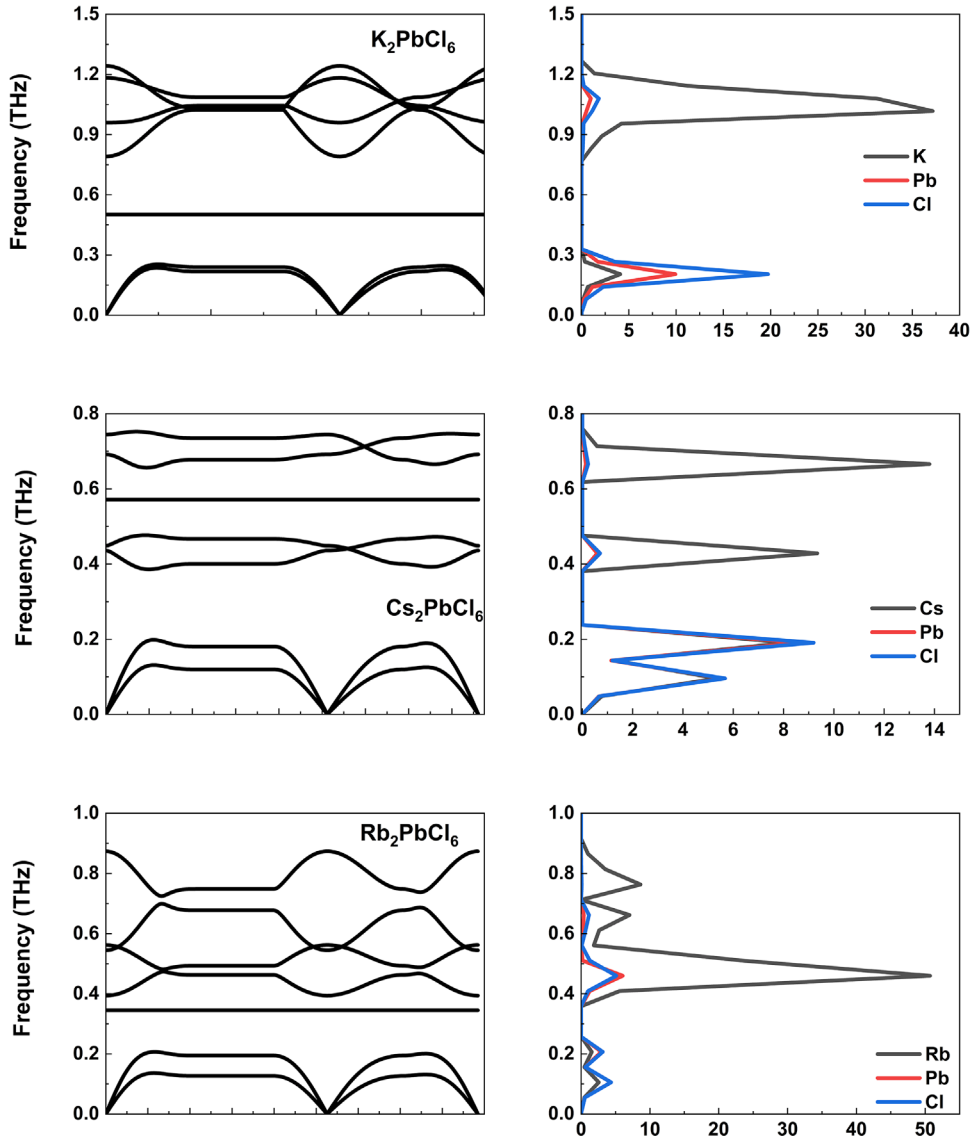

Figure 3. Phonon band structures and PDOS of $(Cs_2, K_2, Rb_2)\ PbCl_6$.

stability.[26] Double perovskites based on lead $(Cs_2, K_2, Rb_2)PbCl_6$, show octahedral distortions in the $PbCl_6$ units, which thus significantly improve their stability, particularly under the influence of pressure and volume. In our current study, we are focused on the analysis of the ideal cubic structure in the study of electronic and mechanical properties. The integration of octahedral distortions into the structural analysis allows a complete understanding of the dynamic behavior of these materials. The improved stability of some double perovskite structures is attributed to the presence of octahedral distortions, this leads to the discovery of new double perovskite materials with improved properties for applications in optoelectronic and thermoelectric devices.

Prasanna et al. report that PbI_6 octahedral tilts in double perovskites control the structuralstability and banding characteristics for solar cell applications.[27] The structure $(Cs_2, K_2, Rb_2)PbCl_6$ was analyzed in the presence of structural distortions, where octahedral inclinationsof $PbCl_6$, cation displacements, and octahedral rotations are cited. Calculations show that the presence of distortions strengthens the bonds between the $PbCl_6$ octahedra and the surrounding cations, thus improving structural stability. This is consistent with Goldschmidt's tolerance factor theory, which suggests that larger cations (*Cs, K, Rb*) fill the spaces around the octahedra, reducing distortions and promoting stability. Additionally, our results indicate that the structural stability in these materials is attributed to the binding interactions between *Cl* and cations (*Cs/Rb/K*). Specifically, our calculations reveal that *Cl—Cs* bonds are stronger than those of *Cl-Rb* and *Cl-K*, contributing to the greater stability of Cs_2PbCl_6 compared to Rb_2PbCl_6 and K_2PbCl_6. This approach is consistent with recent research[25] which states that octahedral tilts bring the anions closer to the central cations, forming stronger bonds

Table 3. Goldschmidt's tolerance factor (t), octahedral factor (μ), and ionic radii for $(Cs_2, K_2, Rb_2)PbCl_6$.

	K_2PbCl_6			Cs_2PbCl_6			Rb_2PbCl_6		
Ionic radii [Å]	r_K	r_{Pb}	r_{Cl}	r_{Cs}	r_{Pb}	r_{Cl}	r_{Rb}	r_{Pb}	r_{Cl}
	1.64	1.72	1.81	1.88	1.72	1.81	1.64	1.72	1.81
Tolerance factor (t)		1.062			1.068			0.965	
Octahedral factor (μ)		0.428			0.428			0.428	

that improve the stability of the perovskite. Based on this analysis, it is concluded that the stability sequence $Cs \rightarrow Rb \rightarrow K$ is due to the size of the cations, structural distortions, and the nature of the bonding interactions between the cations and the chloride species. The bulk modulus B and its pressure derivative B' were obtained from the Birch–Murnaghan equation of state (EOS) and the results are reported in Table 1. The bulk modulus values of Cs_2PbCl_6 and Rb_2PbCl_6 agree with their reported values.[18] There are no values of the lattice constant and bulk modulus for K_2PbCl_6. The bond lengths of nearest neighbors for $(Cs_2, K_2, Rb_2)PbCl_6$ calculated using optimized and experimental lattice constant are listed in **Table 2**. The bond lengths are related to the (Cs, K, Rb) radius. The experiment and theoretical values are in well agreement. The $Cs—Pb$ and $Pb—Cl$ bond lengths are in well agreement with those reported in the literature for Cs_2PbCl_6.[15]

Bond lengths play a key role in material stability, which guides the design of stable optoelectronic semiconductors. Fairly small bond lengths mean that the electrons are more bound to the atom and require more energy to be removed, leading to an increase in the bandgap. Phonon band structures and PDOS of $(Cs_2, K_2, Rb_2)PbCl_6$ are visualized in **Figure 3** in order to study the dynamic stability. No negative frequencies are noted in the spectra, therefore dynamic stability is ensured. In the optical mode, for frequencies located beyond 0.4 THZ for $(Cs_2, K_2, Rb_2)PbCl_6$ two atoms of (Cs, K, Rb) in a unit cell vibrate in an opposite direction, while for the acoustic mode, with frequencies below 0.2 THZ governed by the vibrations of the Cl and Pb atoms in the unit cell, which vibrate in the same direction. The formation enthalpy of $(Cs_2, K_2, Rb_2)PbCl_6$ corresponding to the reaction of formation for these compounds at room temperature from simple elements

Table 4. Elastic moduli, bulk modulus, Debye temperature, averaged sound velocity, Young's modulus, shear modulus, Poisson's ratio computed using Voigt–Reuss–Hill approximation for $(Cs_2, K_2, Rb_2)PbCl_6$.

		K_2PbCl_6	Cs_2PbCl_6	Rb_2PbCl_6
C_{11} [GPa]		11.62	19.35	25.49
Other cal			12.96[18]	
C_{12} [GPa]		6.07	10.52	14.54
Other cal			7.34[18]	
C_{44} [GPa]		5.89	7.96	10.32
Other cal			3.90[18]	
B [GPa]		7.92	13.47	18.19
θ_D [K]		127.52	131.72	158.15
Averaged sound velocity		1369.28	1415.58	1655.88
Bulk modulus	Voigt	7.93	13.47	18.19
	Reuss	7.93	13.47	18.19
	Hill	7.93	13.47	18.19
Shear modulus	Voigt	4.64	6.54	8.38
	Reuss	4.06	6.02	7.62
	Hill	4.35	6.28	8.00
Young modulus	Voigt	11.66	16.89	21.8
	Reuss	10.41	15.73	20.07
	Hill	11.04	16.32	20.94
Poisson ratio	Voigt	0.254	0.290	0.300
	Reuss	0.281	0.300	0.316
	Hill	0.267	0.301	0.301

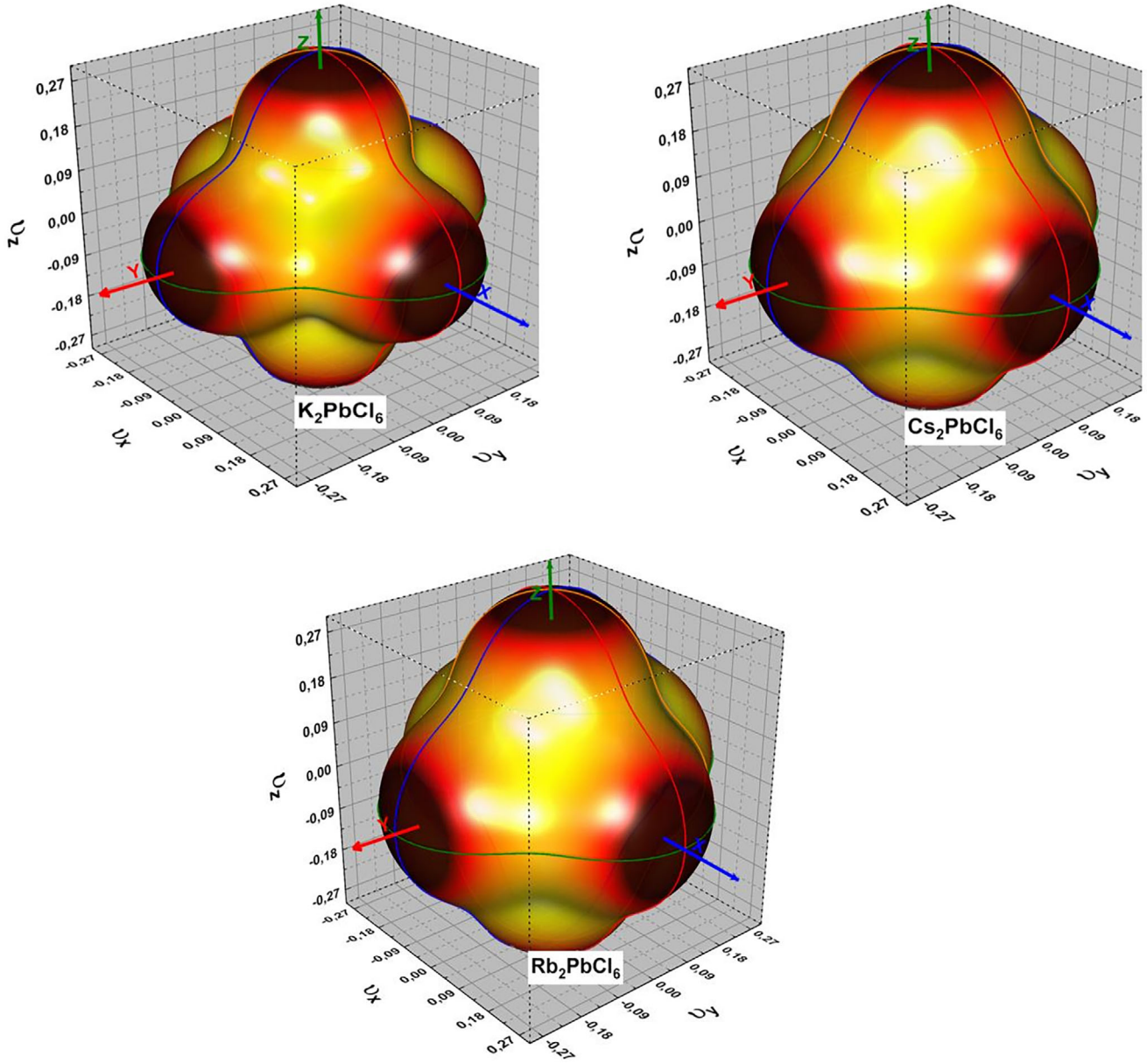

Figure 4. The 3D surface construction of Poisson's ratio in $(Cs_2, K_2, Rb_2)PbCl_6$.

in their most stable molecular form follows this reaction

$$(Cs, K, Rb)PbCl_3 + 2HCl + (Cs, K, Rb)Cl + \frac{1}{2}O_2 \rightarrow (Cs_2, K_2, Rb_2)PbCl_6 + H_2O \quad (1)$$

The formation enthalpy of K_2PbCl_6, Cs_2PbCl_6, and Rb_2PbCl_6 is −2.956, −2.863, and −2.954 eV. It translates the binding force of a solid, and it is the energy needed to dispatch the solid into isolated atoms when all bonds are broken. The negativity of the formation energy of a material reflects its thermal stability and the reaction will be exothermic and conclude the synthesis possibility of all studied double perovskites. Goldschmidt tolerance factor (t) and octahedral factor (u) of $(Cs_2, K_2, Rb_2)PbCl_6$ are given by $t = \frac{(r_{(K,Cs,Rb)}+r_{Pb})}{\sqrt{2}(r_{Pb}+r_{Cl})}$ [28] and $u = \frac{r_{Pb}}{r_{Cl}}$ [29] as reported in **Table 3**, where r_{Pb}, $r_{(K,Cs,Rb)}$, r_{Cl} represent the ionic radii for ions Pb, (K, Cs, Rb) and Cl sites. The double perovskites under study have t and u values close to 1.0 and 0.4, which confirm their structural stability.

3.2. Mechanical Characteristics

The elastic moduli of cubic structure $(Cs_2, K_2, Rb_2)PbCl_6$ are listed in **Table 4**. They verify the criteria $C_{11} + 2C_{12} \rangle 0$, $C_{44} \rangle 0$, $C_{11} - C_{12} \rangle 0$, $C_{12} \langle B \langle C_{11}$, which give guarantee of mechanical stability.

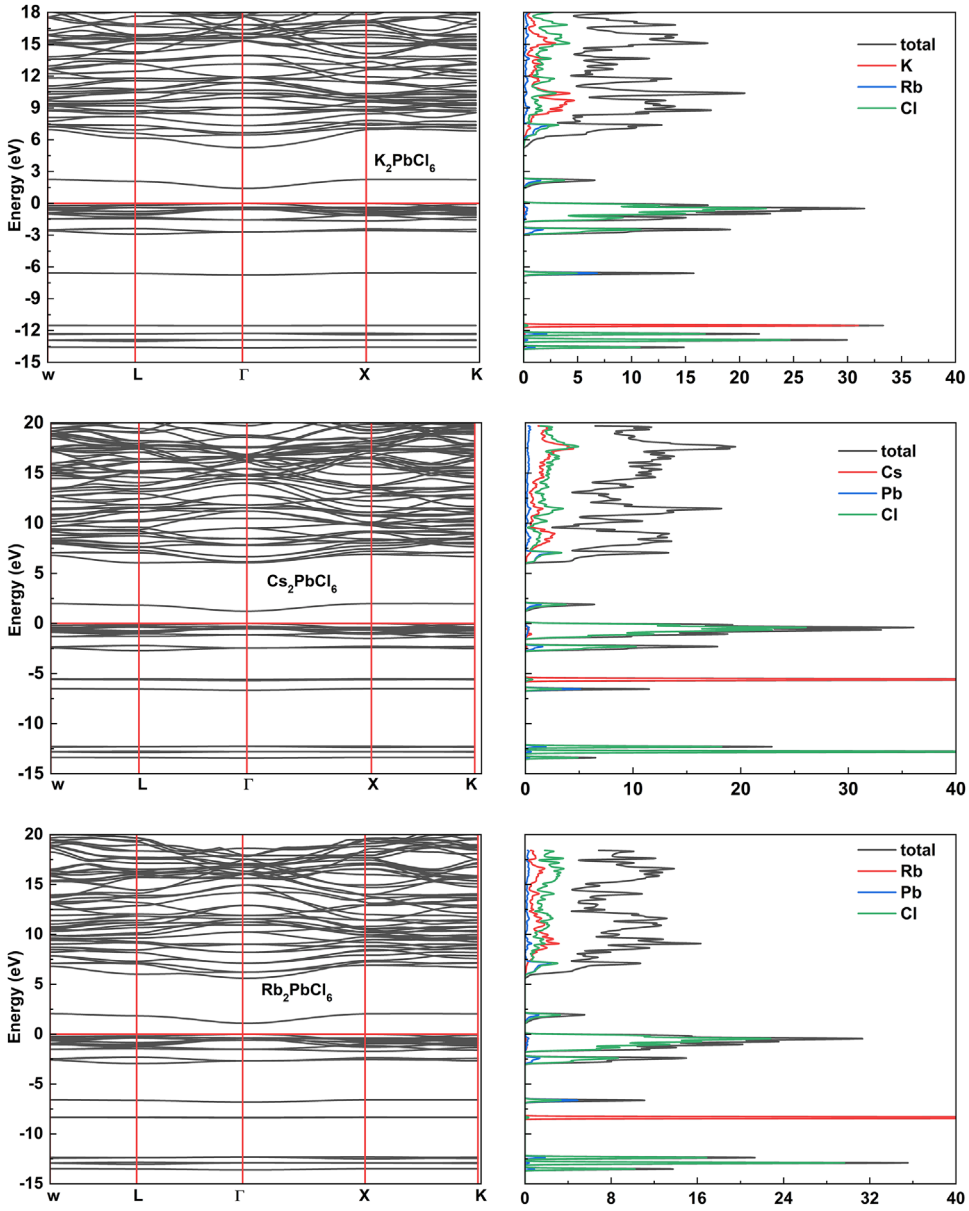

Figure 5. Electronic band structures and density of states of $(Cs_2, K_2, Rb_2)PbCl_6$ using GGA approximation.

Elastic constants are calculated using the stress–strain method. The bulk modulus of elasticity (B), Young's modulus (E), shear modulus (G), and Poisson's ratio (ν) computed with the Voigt–Reuss–Hill (VRH) approximation are reported in Table 4. The weaker elastic moduli leads to their easy deformation and less resistance to stretching or bending and hardness. Young's modulus is the longitudinal modulus of elasticity, which characterizes the resistance of the material to deformation, and the larger the value of Young's modulus, the greater the stiffness of the material. Young's modulus confirms the larger resistance to uniaxial deformation. The values of Poisson's ratio $\nu > 0.25$ support forces as central type in all compounds and the materials exhibit relative toughness. We study the link between hardness and shear modulus and bulk modulus of metal halide double perovskites calculated according to the model[30]

$$H = 2\left(\frac{G^3}{B^2}\right)^{0.585} - 3 \tag{2}$$

Hardness is the resistance of a material to localized plastic deformation. From values reported in Table 4 for shear modulus and bulk modulus, Cs_2PbCl_6, K_2PbCl_6, and Rb_2PbCl_6 show lower hardness. **Figure 4** shows 3D surface of Poisson's ratio for $(Cs_2, K_2, Rb_2)PbCl_6$ double perovskites. It is presented by a contour along each graph in different directions using GGA-mBJ functional. We note that Poisson's ratio is anisotropic. There are

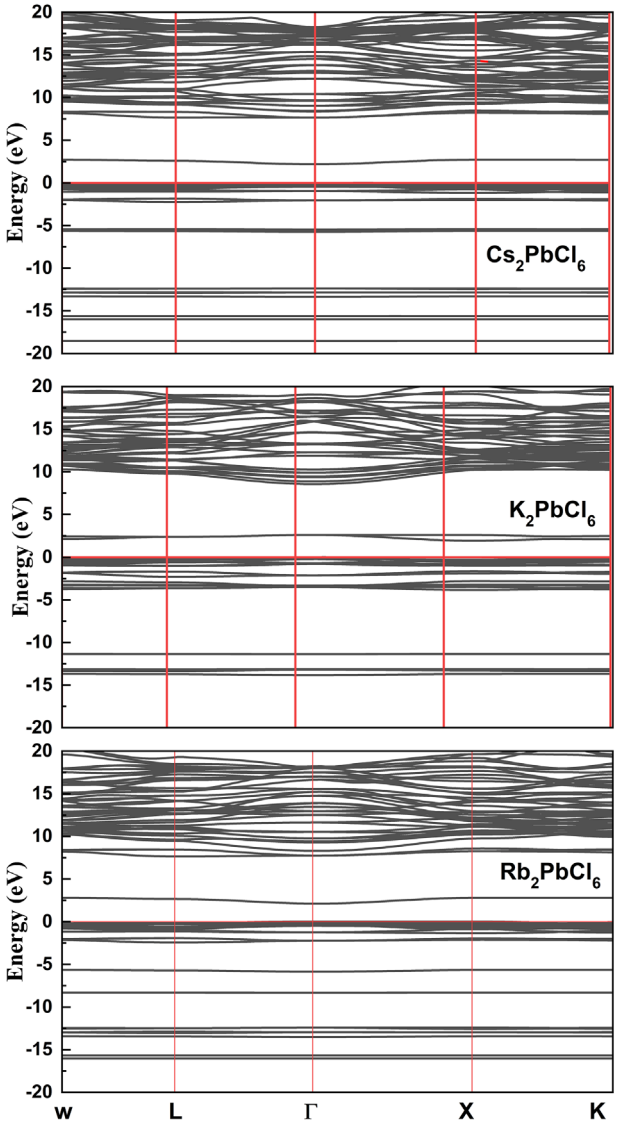

Figure 6. Electronic band structures of $(Cs_2, K_2, Rb_2)PbCl_6$ using mBJ-GGA approximation.

two independent engineering elastic moduli: the shear (G) and the bulk (B) modulus. These quantities can be connected to single crystal elastic constants using different averaging techniques. The shear modulus is an indicator of the mechanical hardness. Whereas, the bulk modulus represents a measure of the average bond strength of the atoms in the crystal, and it is proportional to the cohesive energy.

3.3. Electronic Band Structure and Density of States

The band structure and density of states of double perovskites provide insight into their electronic characteristics. Electronic band structure and density of states using GGA and mBJ-GGA approximations for $(Cs_2, K_2, Rb_2)PbCl_6$ are depicted in **Figures 5** and **6**. The bandgap between the maximum of the valence band and the minimum of the conduction band called the forbidden band defines the absorption edge of a material is direct Γ-Γ on the Brillouin zone. The direct Γ-Γ bandgap of $(Cs_2, K_2, Rb_2)PbCl_6$ using GGA and mBJ-GGA are reported in **Table 5**. The electronic contribution to the first conduction band is mainly due to Cl states in all compounds. The electronic configuration of *Cs*, *K*, and *Rb* are *Cs*: [Xe] $6s^1$, *K*: [Ar] $4s^1$, and *Rb*: [Kr] $5s^1$. The filled states of *Cs*, *K*, and *Rb* contribute to the upper valence band with little contribution of the partially filled $6s^1$, $4s^1$, and $5s^1$ orbitals. Pb atom possess electronic configuration as [Xe] $6s^2$ $4f^{14}$ $5d^{10}$ $6p^2$. The valence band maximum and first conduction band of $(Cs_2, K_2, Rb_2)PbCl_6$ have partially filled $6p^2$ states. The electronic configuration of Cl was [Ne] $3s^2 3p^5$. The 3p-Cl states have play major role in composition of valence band. Also, these states hybridize with 6p-Pb states The fundamental transition takes place between 3p-Cl states and 6p-Pb states. The density of states predicts that all compounds are semiconductors. It is clear that an intermediate band appears in the conduction band of the compounds under study. This band localized at an energy identical to that which corresponds to the start of the absorption of photons and improves the efficiency of these solar cells. Distortions have effects on phases and properties, such as octahedral tilts that affect the bandgap in lead chloride perovskites.[26] The flexible nature of the $PbCl_6$ structure in $(Cs_2, K_2, Rb_2)PbCl_6$ arises from the large metal-halide-metal (Pb—Cl—Pb) bond angle, giving the perovskites another phase transition property, which largely influences the electronic structure. The large coordination number of cations at (*Cs*, *K*, *Rb*) and Pb-sites, the difference of ionic radii and valence electrons cause lattice distortion of the structure, which leads to the reduction of structural symmetry of perovskite, hence these chloride perovskites exhibit outstanding and diverse physical properties. Structural changes that increase the Pb-Cl overlap reduce the bandgap, while structural changes which decrease the overlap of metal halides increase the bandgap.

3.4. Optical Properties

Optical parameters studied to clarify the utility of these compounds include the refractive index, real dielectric function, loss function, and absorption coefficient as reported in **Figure 7**. The information about the refractive index coefficient for optical materials is essential in designing photonic devices. The high refractive index is major factor that limits the output efficiency of solar cells. it can be seen that the static refractive index for Cs_2PbCl_6, K_2PbCl_6, and Rb_2PbCl_6 are 1.8, 1.75, and 1.85, respectively. The maximum refractive index is about 2.3 observed at the ultraviolet (UV) photon energy of 4 eV, then it decreases rapidly to 0.9 at 4.5 eV. In the visible range at 2.25 eV, the refractive index is about 2. In comparison to the refractive index of Si ($n = 3.4$)[31] at the same energy, the double perovskites structures in this study hold a huge advantage over Si for solar cell applications. The static dielectric constant is the sum of the electronic and lattice contributions of electronic thermal conductivity. The electronic component is also called optical dielectric constant ϵ_∞ and it equals the square of the refractive index, $\epsilon_\infty = n^2$. The large static dielectric constant arises from the lattice contribution. The static dielectric constant represents the electronic part of the dielectric

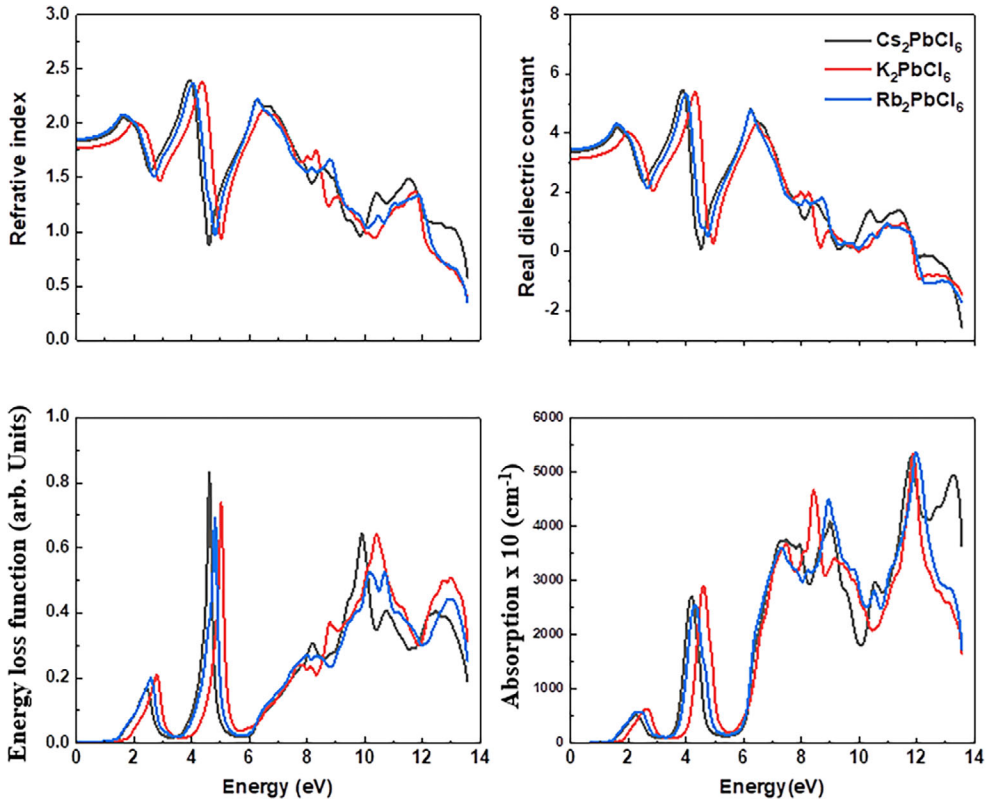

Figure 7. Refractive index, real dielectric constant, energy loss function, and absorption as a function of photon energy for $(Cs_2, K_2, Rb_2)PbCl_6$ using mBJ-GGA functional.

function.[32] The static dielectric constant for Cs_2PbCl_6, K_2PbCl_6, and Rb_2PbCl_6 are3.3, 3.1, and 3.4, respectively. From analysis of dielectric constant, all compounds are capable of absorbing energy in the range 1–5 eV, making it suitable for photovoltaic applications, and particularly for solar energy applications. The electron energy loss function measures the energy dissipated by electrons as they traverse a dielectric material. The strong peak near 5 eV is mainly caused by the bulk plasmon excitation in the ultraviolet light. The present spectra reveal four significant characteristic peaks, exhibiting similar positions (2.5, 5, 10.5, and 13 eV) but quite different intensities. The spectra indicate that the shape excitation is mainly above 5 eV, while the surface excitation mainly influences in the low of the energy loss range. There is no loss below 0.8 eV. At very low energy losses below 1.5 eV, there is no loss and above 6 eV, the precision of the data is compromised due to the broadening of the elastic peak. The double perovskites exhibit large absorption coefficients in the UV (45 000 cm^{-1}) and visible ranges (5000 cm^{-1}). We note that Cs_2PbCl_6 has an absorption coefficient of 1.45×10^5 cm^{-1} at 3.42 eV.[19] The organic–inorganic perovskite MAPbI3, which is one of the most promising perovskites for future solar cells has a maximum reported absorption coefficient of 5.2×10^4 cm^{-1} in the ultraviolet range.[32]

Table 5. The direct Γ-Γ bandgap of $(Cs_2, K_2, Rb_2)PbCl_6$ calculated using GGA and mBJ-GGA functionals.

	E_g [eV] GGA	E_g [eV] mBJ-GGA
K_2PbCl_6	1.406	2.541
Cs_2PbCl_6	1.216	2.181
Rb_2PbCl_6	1.078	2.114

3.5. Thermoelectric Characteristics

Semiconductors with direct bandgap and flat conduction and valence bands exhibit adequate thermoelectric parameters.[19] We show in **Figure 8** the effect of chemical potential shifted with respect to the Fermi energy from −1.2 to 1.2 eV on Seebeck coefficient at temperatures $T = 300$, 600, and 900 K for $(Cs_2, K_2, Rb_2)PbCl_6$. Seebeck coefficient increases with increasing chemical potential. The general trend for $(Cs_2, K_2, Rb_2)PbCl_6$ with increasing temperature is a decrease in Seebeck. Two peaks in the profile are observed for p-type character at a chemical potential around 0–1.2 eV. The maximum Seebeck coefficient obtained is about 1600 μV K^{-1} at 300 K and $E\text{-}E_F = 0.5$ and 0.85 eV. We see that $(Cs_2, K_2, Rb_2)PbCl_6$ have positive values of Seebeck coefficient, which reveals that p-type charge carriers are dominant and increases with increasing temperature for enhancing their performance. The thermal conductivity is a combination of electronic thermal conductivity and phononic thermal conductivity. **Figure 9** shows the electronic thermal conductivity divided by relaxation time as a function of chemical potential at temperatures

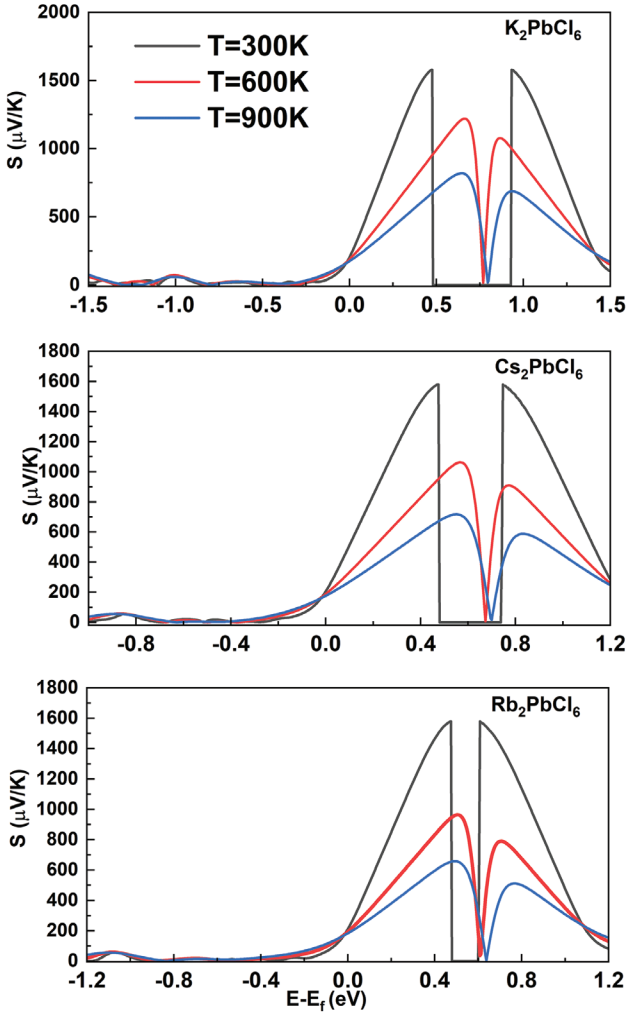

Figure 8. Seebeck coefficient as a function of chemical potential at temperatures $T = 300$, 600, and 900 K for $(Cs_2, K_2, Rb_2)PbCl_6$ using GGA-mBJ.

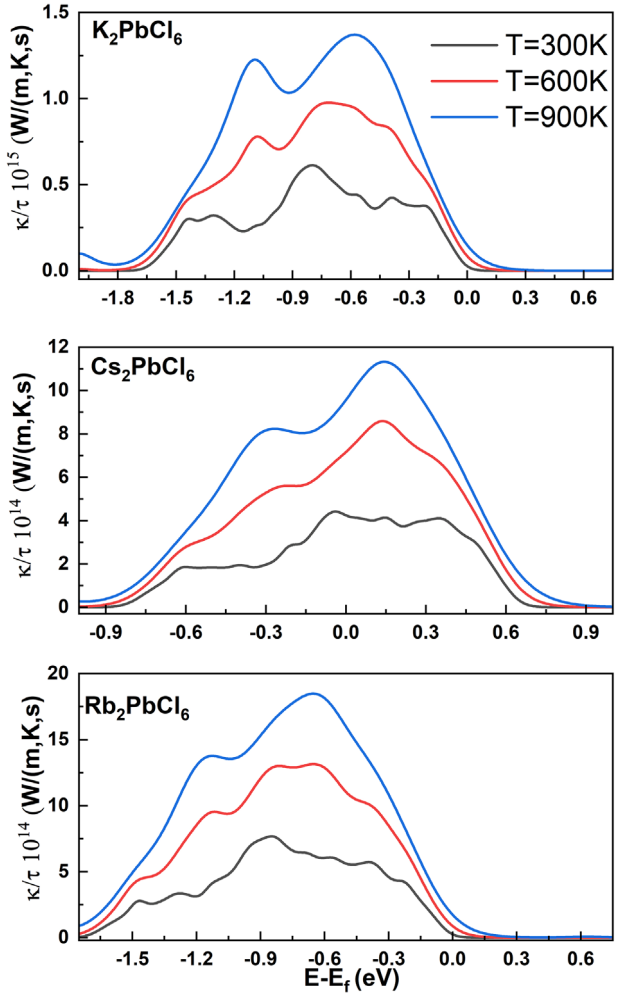

Figure 9. Electronic thermal conductivity as a function of chemical potential at temperatures $T = 300$, 600, and 900 K for $(Cs_2, K_2, Rb_2)PbCl_6$ using GGA-mBJ.

$T = 300$, 600, and 900 K. Thermal conductivity is a parameter for identifying materials intended for technological applications, such as thermoelectric conversion. A high-performance thermoelectric material has low thermal conductivity. Cs_2PbCl_6 have positive values of thermal conductivity and this enhances their performance as n-type and p-type. The high value is obtained at p-type character. While $(Rb_2, K_2)PbCl_6$ have positive values for n-type character. Better performance requires the use of low temperature. Thermal conductivity decreases with increasing defects. The dependence of thermal conductivity on temperature in the low temperature region is small. The electronic thermal conductivity enhanced their performance as n-type and p-type. The variation of electrical conductivity divided by relaxation time (σ/τ) as a function of chemical potential from −2 to 1 eV at temperatures 300, 600, and 900 K for $(Cs_2, K_2, Rb_2)PbCl_6$ using mBJ-GGA is shown in **Figure 10**. Cs_2PbCl_6 has positive values of thermal conductivity and this enhances their performance as n-type and p-type. While $(K_2, Rb_2)PbCl_6$ have positive value only for n-type character. The electrical conductivity for negative chemical potential is higher in $(K_2, Rb_2)PbCl_6$, while Cs_2PbCl_6 possessed positive electrical conductivity for n-type and p-type character. The average power factor is plotted against the chemical potential at 300, 600, and 900 K as illustrated in **Figure 11**. The positive (negative) chemical potential scale indicates the electron (hole) concentration, respectively. The power factor is maximum near $\mu = -1.2$ eV for K_2SnCl_6 and at $\mu = 0$ eV, attributed to significant increment in the electrical conductivity at high electron concentration level. Power factor increases with increasing temperature. The large magnitude of power factor is obtained in the case of large electrical conductivity. Consequently, $(Cs_2, K_2, Rb_2)PbCl_6$ exhibit good thermoelectric response at the higher temperatures.

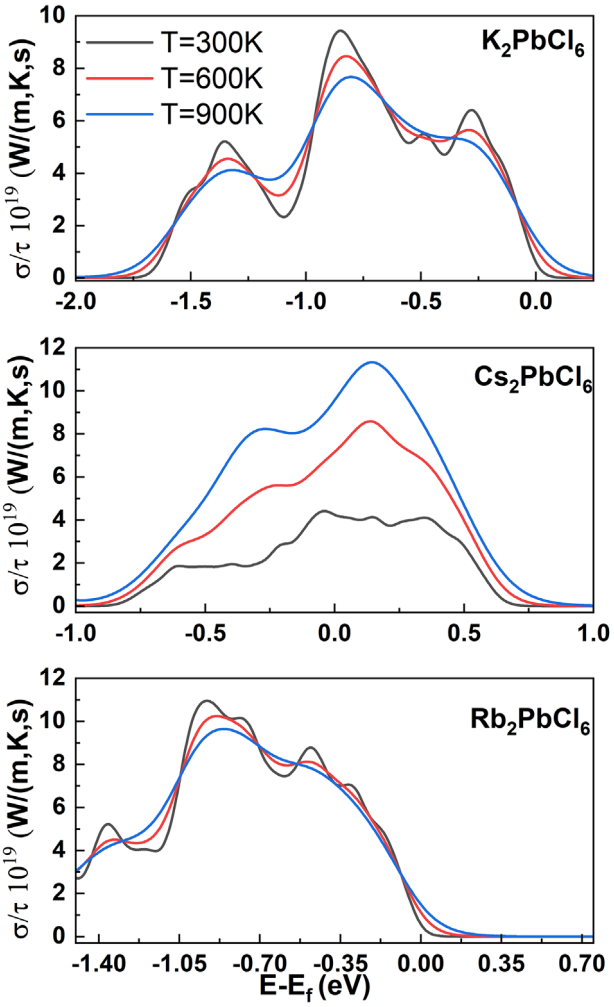

Figure 10. Electrical conductivity as a function of chemical potential at temperatures $T = 300$, 600, and 900 K for $(Cs_2, K_2, Rb_2)PbCl_6$ using GGA-mBJ.

4. Conclusion

We performed a comprehensive analysis of stability, mechanical, optoelectronic, and thermoelectric characteristics for $(Cs_2, K_2, Rb_2)PbCl_6$ using GGA and mBJ-GGA as implemented in Wien2K code. These lead-based double perovskites are quite suitable for solar cells and optoelectronic applications, owing to their direct bandgaps smaller than their respective single perovskites structures $(Cs_2, K_2, Rb_2)PbCl_6$. The electrical conductivity for negative chemical potential is higher in $(K_2, Rb_2)PbCl_6$, while Cs_2PbCl_6 has positive electrical conductivity for n-type and p-type character. The large magnitude of power factor is obtained for high temperature and large electrical conductivity, consequently, $(Cs_2, K_2, Rb_2)PbCl_6$ exhibit good thermoelectric response at higher temperatures. They exhibit high absorption coefficients and dielectric constants in the ultraviolet and visible energy ranges, then these double perovskites are quite suitable for applications in solar cell structures. The strong peak near 5 eV for loss function is mainly caused by the bulk plasmon excitation in the ultraviolet light.

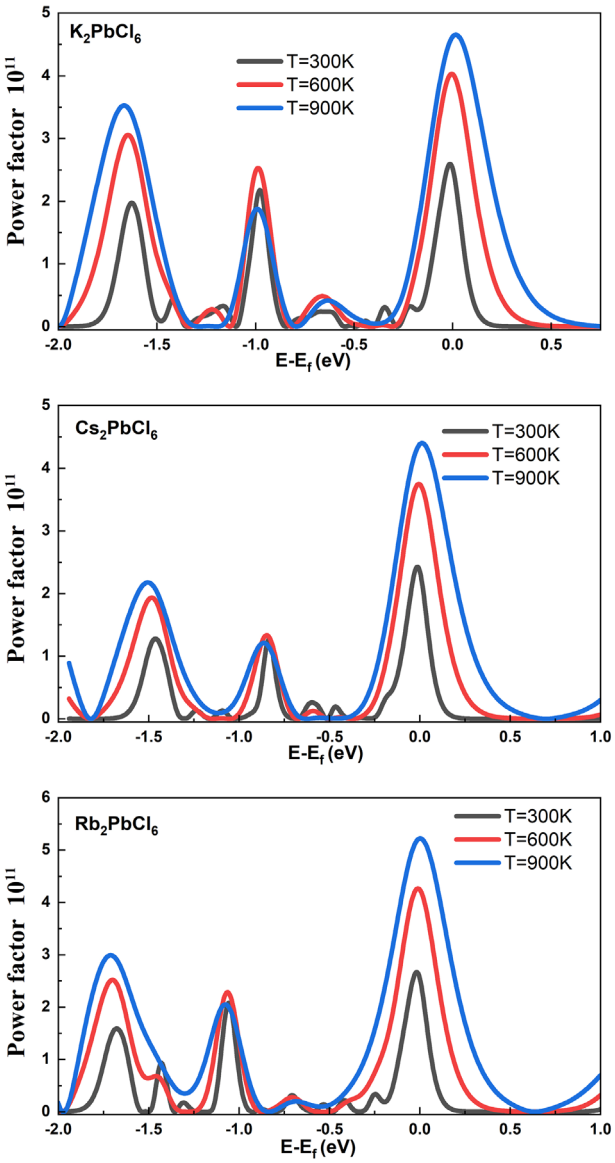

Figure 11. Power factor as a function of chemical potential at temperatures $T = 300$, 600, and 900 K for $(Cs_2, K_2, Rb_2)PbCl_6$ using GGA-mBJ.

Acknowledgements

The authors extended their appreciation to the Deanship of Scientific Research at Northern Border University, Arar, KSA for funding this research work through the Project No. NBU-FFR-2024-310-07.

Conflict of Interest

The authors declare no conflict of interest.

Data Availability Statement

The data that support the findings of this study are available from the corresponding author upon reasonable request.

Keywords

intermediate band, lead-based double perovskites, mBJ-GGA, solar cells, thermal conductivity

Received: August 30, 2024
Revised: November 22, 2024
Published online:

[1] X. Qing, C. Wu, X. Han, *Molecules* **2023**, *28*, 3593.
[2] L. A. Castriotta, E. Calabrò, F. Di Giacomo, S. H. Reddy, D. Takhellambam, B. Paci, A. Generosi, L. Serenelli, F. Menchini, L. Martini, M. Tucci d, A. D. Carlo, *Nano Energy* **2023**, *109*, 108268.
[3] T. Chihi, M. Fatmi, M. A. Ghebouli, B. Ghebouli, H. Djemai, *Chin. J. Phys.* **2017**, *55*, 674.
[4] F. H. Gourji, D. Velauthapillai, *Molecules* **2021**, *26*, 2010.
[5] G. Shao, S. Liu, L. Ding, Z. Zhang, W. Xiang, X. Liang, *Chem. Eng. J.* **2019**, *375*, 122031.
[6] H. Lian, Y. Li, K. Sharafudeen, W. Zhao, G. R. Krishnan, S. Zhang, J. Qiu, K. Huang, G. Han, *Adv. Mater.* **2020**, *32*, 2002495.
[7] H. C. Yoon, S. Lee, J. K. Song, H. Yang, Y. R. Do, *ACS Appl. Mater. Interfaces* **2018**, *10*, 11756.
[8] D. Chen, S. Yuan, J. Chen, J. Zhong, X. Xu, *J. Mater. Chem. C* **2018**, *6*, 12864.
[9] G. Z. Shao, Y. Zhao, Y. X. Yu, H. S. Yang, X. D. Liu, Y. J. Zhang, W. D. Xiang, X. J. Liang, *J. Mater. Chem. C* **2019**, *7*, 13585.
[10] L. Kong, X. Zhang, Y. Li, H. Wang, Y. Jiang, S. Wang, M. You, C. Zhang, T. Zhang, S. V. Kershaw, W. Zheng, Y. Yang, Q. Lin, M. Yuan, A. L. Rogach, X. Yang, *Nat. Commun.* **2021**, *12*, 1246.
[11] Y. Gao, Y. Wu, H. Lu, C. Chen, Y. Liu, X. Bai, L. Yang, W. W. Yu, Q. Dai, Y. Zhang, *Nano Energy* **2019**, *59*, 517.
[12] M. Gong, R. Sakidja, R. Goul, D. Ewing, M. Casper, A. Stramel, A. Elliot, J. Z. Wu, *ACS Nano* **2019**, *13*, 3714.
[13] X. Wang, M. Shoaib, X. Wang, X. Zhang, M. He, Z. Luo, W. Zheng, H. Li, T. Yang, X. Zhu, L. Ma, A. Pan, *ACS Nano* **2018**, *12*, 6170.
[14] S. F. Hoefler, G. Trimmel, T. Rath, *Chem. Chem. Mon.* **2017**, *148*, 795.
[15] I. H. Al-Lehyani, *Arab. J. Chem.* **2021**, *14*, 102920.
[16] Y. Lin, B. Xia, S. Hu, Z. Liu, X. Huang, Z. Xiao, K. Du, *J. Mater. Sci.* **2022**, *57*, 18266.
[17] Y. Yu, Y. Zhou, Y. Zhang, Y. Zhang, X. Liu, X. Liang, J. Liu, S. Chen, W. Xiang, *J. Lumin.* **2021**, *236*, 118129.
[18] H. Peng, R. Sa, D. Liu, *J. Solid State Chem.* **2022**, *310*, 123055.
[19] M. Hussain, M. Rashid, A. Ali, M. F. Bhopal, A. S. Bhatti, *Ceram. Int.* **2020**, *46*, 21378.
[20] B. Ghebouli, M. A. Ghebouli, T. Chihi, M. Fatmi, S. Boucetta, M. Reffas, *Solid State Commun.* **2009**, *149*, 2244.
[21] R. Boudissa, Y. Madkour, T. Chihi, M. A. Ghebouli, H. Bouandas, F. Benlakhdar, M. Fatmi, B. Ghebouli, M. D. Albaqami, S. Mohammad, M. Habila, M. Sillanpää Comput, *Theor. Chem.* **2024**, *1239*, 114792.
[22] J. P. Perdew, K. Burke, M. Ernzerhof, *Phys. Rev. Lett.* **1996**, *77*, 3865.
[23] K. Bouferrache, L. Krache, M. A. Ghebouli, B. Ghebouli, S. I. Ahmed, M. Fatmi, T. Chihi, B. Gueridi, *Chem. Phys. Impact* **2022**, *5*, 100110.
[24] G. Engel, *Z. Kristallogr.* **1935**, *90*, 341.
[25] C. Fang, H. Wang, S. Shi, *J. Materiom.* **2024**, *10*, 304.
[26] C. Fang, H. Wang, S. Shi, *J. Materiom.* **2024**, *10*, 293.
[27] R. Prasanna, A. Gold-Parker, T. Leijtens, B. Conings, A. Babayigit, H.-G. Boyen, M. F. Toney, M. D. McGehee, *J. Am. Chem. Soc.* **2017**, *139*, 11117.
[28] V. M. Goldschmidt, *Die Naturwiss.* **1926**, *14*, 477.
[29] C. Li, K. C. K. Soh, P. Wu, *J. Alloys Compd.* **2004**, *372*, 40.
[30] Y. Liu, C. Fang, S. Lin, G. Liu, B. Zhang, H. Shi, N. Yang, F. Zhang, X. Guo, X. Liu, *Molecules* **2023**, *28*, 7643.
[31] M. Stetsenko, S. Pullano, S. P. Rudenko, L. S. Maksimenko, A. S. Fiorillo, *Electron. Lett.* **2018**, *54*, 331.
[32] R. Singh, P. Singh, G. Balasubramania, *Comput. Mater. Sci.* **2022**, *213*, 111649.